# 6 Photoluminescent Carbon Nanomaterials: Properties and Potential Applications

Yaping Sun, Fushen Lu, Xin Wang, Li Cao, Yi Lin, Mohammed J. Meziani, Haifang Wang, Pengju G. Luo, Bing Zhou, Barbara A. Harruff, Wei Wang, L. Monica Veca, Puyu Zhang, Suyuan Xie, Hua Yang

Department of Chemistry and Laboratory for Emerging Materials and Technology, Clemson University, Clemson, SC 29634-0973, USA

**Abstract** Carbon nanoparticles and nanotubes upon surface passivation or modification via chemical functionalization exhibit strong photoluminescence in the visible and into the near-IR. In this Chapter, the general features and related optical characteristics of the photoluminescence are highlighted, mechanistic issues discussed, and their potential material and biomedical applications explored. For single-walled carbon nanotubes, the similarities and differences between the defect-derived emission and the band-gap fluorescence (emission from individualized single-walled carbon nanotubes) are also discussed.

## 6.1 Introduction

Carbon nanomaterials, especially fullerenes and carbon nanotubes, have attracted much interest for their novel properties and potential technological and biological applications (Baugh man et al., 2002). Much effort has been devoted to the study and understanding of their photoexcited states and related optical characteristics. As predicted theoretically, the electronic states in semiconducting single-walled carbon nanotubes (SWNTs) are characterized by sharp spikes in the density of states (DOS) (Dressel haus et al., 1996). Experimentally, electronic transitions in these nanotubes are featured as broad absorption bands in the near-infrared region, corresponding to the first ($S_{11}$) and second ($S_{22}$) van Hove singularity pairs (Kataura et al., 1999). The band-gap fluorescence mirroring the $S_{11}$ absorption band was reported and studied first by O'Connell, et al. and then by a number of other research groups for SWNTs mostly produced from the high-pressure carbon monoxide disproportionation (HiPco) process (O'Connell et al., 2002;

(1) Corresponding e-mail: syaping@clemson.edu

Bachilo et al., 2002; Lebedkin et al., 2003a, 2003b; Jones et al., 2005; Graff et al., 2005; Lefebvre et al., 2004). An accurate quantum yield value for the fluorescence is still being determined or decided, with current numbers ranging from 0.001% to 0.1% presumably depending on the degree of nanotube bundling/aggregation, surface doping, etc. (O'Connell et al., 2002; Bachilo et al., 2002; Lebedkin et al., 2003a, 2003b; Jones et al., 2005; Graff et al., 2005). There is apparently a required condition for the observation of band-gap fluorescence in SWNTs, namely, that the nanotubes must be dispersed very well to minimize inter-nanotube quenching effects (O'Connell et al., 2002; Bachilo et al., 2002; Graff et al., 2005). Recently, there were reports on the detection of band-gap fluorescence for suspended SWNTs in ambient environment (Lefebvre et al., 2004) and also for nanotubes produced by the laser ablation method (Lebedkin et al., 2003a, 2003b; Hennrich et al., 2005; Arnold et al., 2004).

Even before the first report on band-gap fluorescence from semiconducting SWNTs, carbon nanotubes including both single-walled and multiple-walled ones (MWNTs) upon their surface modification or functionalization were found to be strongly emissive in visible and near-infrared regions (Riggs et al., 2000). In that report, Sun and coworkers referred the emission as luminescence because the nature of the emissive excited state was not well-defined or understood. The luminescence was bright, with quantum yields more than 10% under some conditions (Riggs et al., 2000). While there were questions on the assignment of the strong emission to carbon nanotube species (Zhao et al., 2001), several other research groups confirmed the observation and assignment in subsequent investigations (Guldi et al., 2002; Banerjee and Wong, 2002). For example, Guldi and coworkers reported that the luminescence was associated with carbon nanotube samples from different production methods, including laser ablation and arc discharge, and with heavily oxidized nanotubes (Guldi et al., 2002). Similarly, Wong and coworkers reported strong visible luminescence from carbon nanotubes that are functionalized with Wilkinson's catalyst (Banerjee and Wong, 2002). Mechanistically, Sun and coworkers suggested that the broad visible luminescence could be attributed to the presence of passivated surface defects on carbon nanotubes, which serve as trapping sites for the excitation energy. The passivation as a result of the surface modification and functionalization with oligomeric and polymeric species stabilizes the emissive sites in their competition with other excited state deactivation pathways (Riggs et al., 2000; Sun et al., 2002; Lin et al., 2005).

Recently, mechanistically similar photoluminescence was found and reported in surface-passivated small carbon particles (Sun et al., 2006). These photoluminescent carbon particles, which are being compared with fluorescent semiconductor quantum dots (QDs) (Chan and Nie, 1998; Klimov et al., 2000; Bruchez et al., 1998) are dubbed carbon dots (Sun et al., 2006). The carbon dots offer potentially benign (non-toxic or less toxic) alternatives to currently best performing but mostly heavy metal-based QDs (Esteves and Trindade, 2002; Green, 2002). On the

other hand, the defect-derived luminescence of surface-modified or functionalized carbon nanotubes represents an interesting optical property of the nanotubes because surface defects should be considered as the norm rather than exception in typical SWNTs and MWNTs. These carbon nanomaterials of vastly different aspect ratios and other properties (such as optical polarization characteristics) may find many applications complementarily, such as luminescence imaging with visible and near-infrared colors, sensors based on luminescence quenching properties, and other uses in biological systems in vitro and in vivo. In this article, we will discuss the characteristics of the photoluminescence in carbon dots and surface-modified or functionalized carbon nanotubes, and some mechanistic and application relevant issues.

## 6.2 Photoluminescent Carbon Particles-Carbon Quantum Dots

The finding and development of carbon dots are against the backdrop of rapid advances in the synthesis, property control, and applications of traditional semiconductor QDs (Klimov et al., 2000; Bruchez et al., 1998; Alivisatos, 1996; Larson et al., 2003; Michalet et al., 2005; Parak et al., 2003; Medintz et al., 2005; Kim et al., 2004), and the continued search for alternative QDs based on non-toxic elements (Ding et al., 2002; Chen et al., 2006; Bharali et al., 2005; Seydack, 2005; Wilson et al., 1993; Burns et al., 2006). Traditional QDs are often composed of atoms from groups Ⅱ – Ⅵ or Ⅲ – Ⅴ elements in the periodic table, and are defined as particles with physical dimensions smaller than the exciton Bohr radius (a few nanometers in general) (Chan and Nie, 1998). Several characteristics resulted from the quantum confinement distinguish QDs from traditional fluorophores, such as broad excitation spectra, size-tunable emission properties, longer emission lifetimes, photostability, etc., which are expected to offer substantial advantages in a wide variety of promising applications, especially those in biology and medicine (Michalet et al., 2005). For both in vitro and in vivo uses, however, the known toxicity and potential environmental hazard associated with many of these materials may represent serious limitations (Michalet et al., 2005; Derfus et al., 2004; Kirchner et al., 2005; Lovric et al., 2005). Therefore, the search for benign nanomaterials of similar optical properties continues (Bharali et al., 2005; Seydack, 2005; Wilson et al., 1993; Burns et al., 2006). For quantum-sized silicon, the discovery of Brus and coworkers (Wilson et al., 1993) on the strong luminescence in surface-oxidized nanocrystals has attracted extensive investigations of silicon nanoparticles and nanowires (Holmes et al., 2000; Belomoin et al., 2002; Hua et al., 2005; Li and Ruckenstein, 2004; Huisken et al., 2002). For example, silicon nanoparticles capped with water-soluble polymers, thus compatible with physiological media, have been studied for the

luminescence labeling of cells (Li and Ruckenstein, 2004).

Sun and coworkers (Sun et al., 2006) found and reported carbon-based QDs or carbon dots, which are nanoscale carbon particles with simple surface passivation to exhibit strong photoluminescence in both solution and the solid-state. The emission spectral features and properties of the available carbon dots are comparable to those of surface-oxidized silicon nanocrystals. The starting pristine carbon nanoparticles can be produced from the laser ablation of a graphite target in inert atmosphere under reduced pressure (Lin et al., 2003). Raman spectra of the as-produced samples (Fig. 6.1) are characterized by the typical tangential mode peak (G-band) at 1590 $cm^{-1}$ and the disorder band (D-band) centered at 1320 $cm^{-1}$. The former is related to the graphitic $sp^2$ carbons, while the latter is usually associated with the disorder or defect $sp^3$ carbons. The comparable intensities of the two peaks (the D-band slightly higher) and their broadness suggest that these carbon nanoparticles are largely amorphous. This is supported by results from transmission electron microscopy (TEM) and X-ray diffraction (XRD) analyses of the carbon particles.

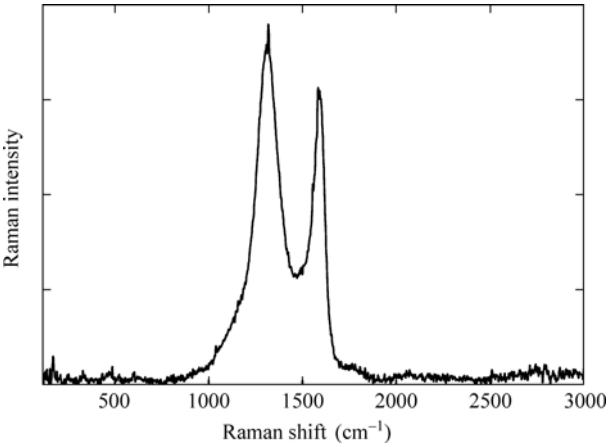


**Figure 6.1** Raman spectrum of carbon nanoparticles (633 nm excitation) shows contributions of both $sp^2$ (G-band at 1590 $cm^{-1}$) and $sp^3$ carbons (D-band at 1320 $cm^{-1}$) (Reproduced from (Sun et al., 2006) with permission. Copyright ©2006 American Chemical Society)

The carbon nanoparticles as produced or after treatments such as refluxing with nitric acid are largely aggregated. They are non-emissive either in the solid state or in suspensions. However, upon simple surface passivation by attaching organic molecules, the particles become soluble in common organic solvents and/or water depending upon the attached functionalities. For example, the use of a diamine-terminated oligomeric polyethylene glycol ($PEG_{1500N}$, Fig. 6.2) or an aminopolymer poly(propionylethylenimine-*co*-ethylenimine) (PPEI-EI, Fig. 6.2) for the surface passivation imparts solubility in both water and chloroform. Microscopy results (Fig. 6.3) suggest that these soluble surface-modified carbon

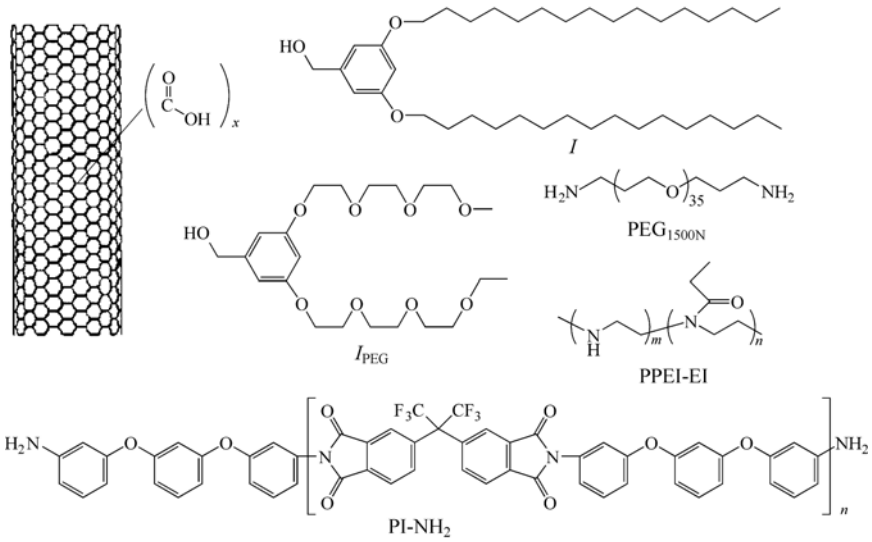


**Figure 6.2** Defect-derived functionalization of carbon nanotubes

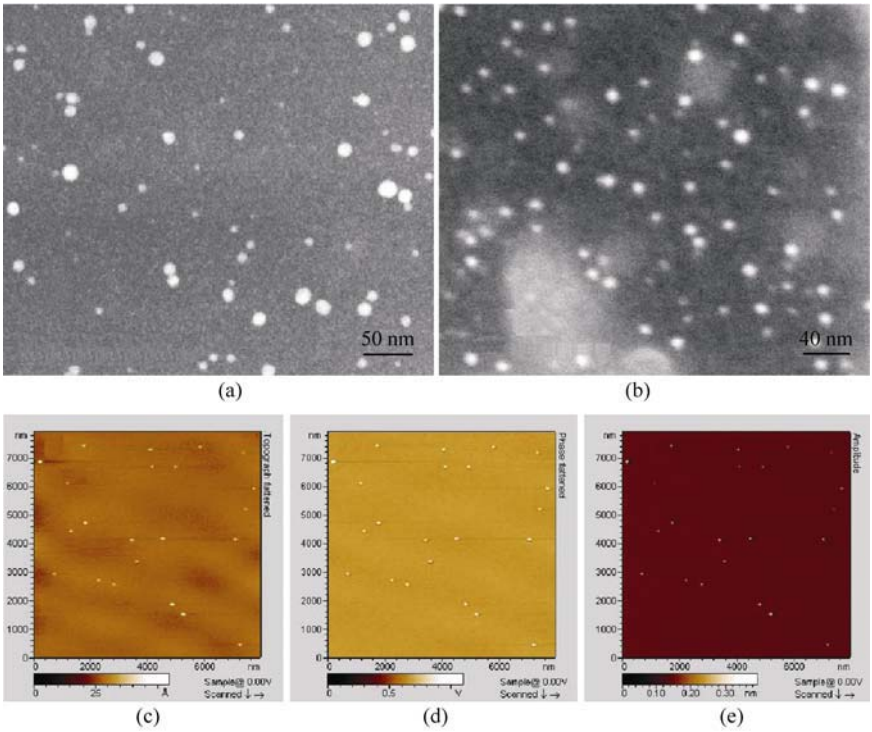


**Figure 6.3** Representative S-TEM images (Color Fig. 13) of carbon dots surface-passivated with (a) $PEG_{1500N}$ and (b) PPEI-EI, and AFM images of carbon dots surface-passivated with PPEI-EI (c) topography, (d) phase, and (e) amplitude. (Reproduced from (Sun et al., 2006) with permission. Copyright ©2006 American Chemical Society)

nanoparticles are well dispersed as individual particles with diameters of a few nanometers.

The surface passivation makes carbon nanoparticles into carbon dots, which exhibit bright and colorful photoluminescent in the visible to the near infrared (Sun et al., 2006) (Fig. 6.4). Since the organic functional groups are colorless and non-emissive in the wavelength ranges, the emission must be due to the passivated carbon nanoparticles (carbon dots). Mechanistically, the photoluminescence may be attributed to the presence of surface energy traps, likely related to the abundant surface defect sites that become emissive upon passivation. It should be noted that surface passivation is also required in the luminescent silicon nanocrystals, though the emissions there were widely attributed to band-gap transitions (radiative recombination of excitons).

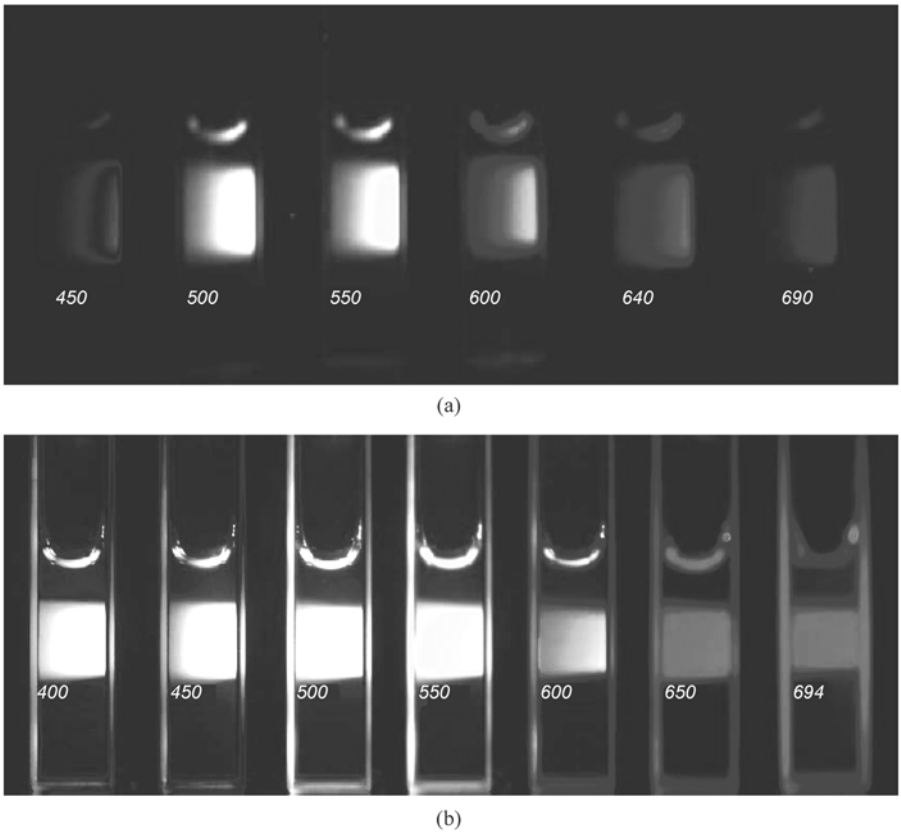


**Figure 6.4** Aqueous solutions of the $PEG_{1500N}$-attached carbon dots (Color Fig. 14) (a) excited at 400 nm and photographed through band-pass filters of different wavelengths as indicated, and (b) excited at the indicated wavelengths and photographed directly (Reproduced from (Sun et al., 2006) with permission. Copyright ©2006 American Chemical Society)

Nevertheless, the surface emissive sites of the carbon dots are likely quantum confined in the sense that a large surface-to-volume ratio is required for the strong photoluminescence. In fact, larger carbon particles (30 – 50 nm in diameter) with the same surface passivation are much less luminescent (Sun et al., 2006).

Photoluminescence spectra of carbon dots are generally broad and dependent on excitation wavelengths, moving progressively to the red as the excitation wavelength becoming longer (Fig. 6.5). As in silicon nanocrystals (Wilson et al., 1993) and some other nanoscale optical materials (Riggs et al., 2000; Bruchez et al., 1998), such emission characteristics are indicative of the inhomogeneity in underlying emissive species. There are not only particles of different sizes in the sample but also a distribution of different emissive sites on each carbon dot (Sun et al., 2006).

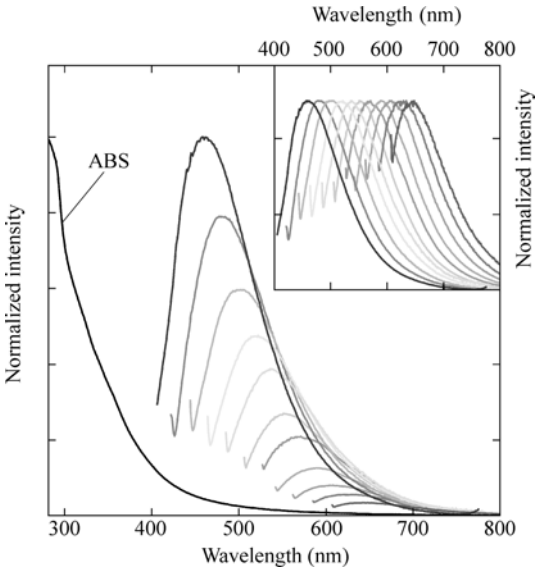


**Figure 6.5** The absorption spectrum (ABS) and emission spectra (with progressively longer excitation wavelengths from 400 nm on the left in 20 nm increment) of PPEI-EI-carbon dots in an aqueous solution. The emission spectral intensities are normalized to quantum yield (normalized to spectral peaks in the inset) (Reproduced from (Sun et al., 2006) with permission. Copyright ©2006 American Chemical Society)

The reported carbon dots have photoluminescence quantum yields from about 4% to more than 10% at 400 nm excitation, and the yields decrease progressively with longer excitation wavelengths. The observed emission quantum yields are obviously dependent on how well is the surface passivation in the carbon dots. When the dots with relatively lower quantum yields are subject to a repeat of the same surface passivation reaction, they become more emissive with higher quantum yields.

The luminescence decays of carbon dots can be measured by using the time-correlated single photon counting (TCSPC) technique. The observed decays are generally not mono-exponential. When fitted with multi-exponential functions, the average lifetimes of the carbon dots are on the order of 4 – 5 ns.

The photoluminescence of carbon dots is stable against photobleaching in irradiation with a 450-W xenon lamp for hours. There is also no blinking in the photoluminescence (Fig. 6.6), in contrast to the commonly observed fluorescence blinking in many other QDs (such as CdSe (Kuno et al., 2001; Shimizu et al., 2001), InP (Kuno et al., 2001), Si (Sychugov et al., 2005) and Au (Geddes et al., 2003).

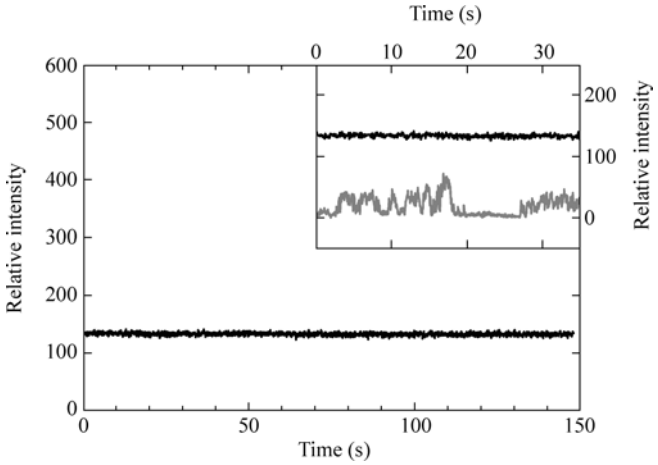


**Figure 6.6** The time-dependence of luminescence intensity of $PEG_{1500N}$-carbon dots measured in confocal microscopy (Leica TCS SP2, the frame rate 37 ms/ frame at 514 nm excitation). Shown in the inset is a comparison of the same data (black) with that (grey) of a commercially available blinking gold nanoparticle sample (Ted Pella, Inc, diameter ~50 nm). (Reproduced from (Sun et al., 2006) with permission. Copyright ©2006 American Chemical Society)

In summary, carbon dots are potentially competitive alternatives to traditional semiconductor QDs. Carbon as an element is obviously non-toxic and environmentally benign. With further improvement in performance, carbon dots will likely find many applications in biology and medicine, especially those that require photoluminescent labels in vivo.

## 6.3 Photoluminescent Carbon Nanotubes

Carbon nanotubes typically contain surface defects that structurally resemble the surface of a nanoscale carbon particle, and may thus be made brightly photoluminescent just like carbon dots (Riggs et al., 2000; Guldi et al., 2003; Banerjee and Wong, 2002; Sun et al., 2002; Lin et al., 2005; Sun et al., 2003;

Zhou et al., 2006; Kose et al., 2006). In fact, it took almost a decade since the discovery of carbon nanotubes to the realization that these nanotubes are in fact strongly luminescent under well-defined conditions (Riggs et al., 2000). The revealing of the luminescence was a direct result of the significant advance in the chemical modification and functionalization of carbon nanotubes for their solubilization and dispersion at the individual nanotube level (Lin et al., 2005; Sun et al., 2002).

### 6.3.1 A Consequence of Functionalization

As-produced carbon nanotubes are generally insoluble in common organic solvents and water (Bahr et al., 2001). The insolubility is due to the fact that these species are relatively large in sizes and also significantly bundled (strong van der Waals interactions between adjacent nanotube graphitic surfaces). The bundling of nanotubes has made it difficult to observe many of their intrinsic properties, including the band-gap fluorescence and the defect-derived luminescence due to their sensitivity to inter-nanotube quenching (O'Connell et al., 2002; Riggs et al., 2000).

The field of chemical functionalization of carbon nanotubes has become very active and diversified, driven primarily by application needs in the processing of nanotube-based materials. The functionalization leads to the homogeneous dispersion (the exfoliation of nanotube bundles, especially for SWNTs) and solubilization of the nanotubes. The chemical functionalization methods may be classified roughly into two categories, i.e. noncovalent and covalent modifications (Sun et al., 2002; Bahr and Tour, 2002; Hirsch, 2002; Tasis et al., 2003; Niyogi et al., 2002). The noncovalent functionalization methods usually take advantage of the hydrophobic or π-π interactions between functional molecules (such as surfactants and some polymers) and the nanotube surface. The reagents in covalent methods target either the nanotube graphitic sidewall (Bahr et al., 2002; Hirsch, 2002; Tasis et al., 2003) or surface defect sites (carboxylic acid moieties from oxidative acid treatment of the defect carbons on nanotubes, see below) (Sun et al., 2002; Niyogi et al., 2002). Compared to noncovalent functionalization, covalent methods have provided a higher degree of flexibility in functional groups selection and generally higher efficiency in the resulting nanotube dispersion and solubilization.

The nanotube sidewall chemistry is largely derived from the previously well-developed graphite and fullerene chemistry, since the reactivity of nanotube $sp^2$ carbons, as a result from π-orbital misalignment and curvature-induced pyramidalization, is in fact intermediate between those two carbon allotropes (Niyogi et al., 2002). A less attractive feature with the dispersion and solubilization via the sidewall chemistry in some applications is that it disrupts the nanotube graphitic surface and thus alters the nanotube electronic structures, again making it difficult to observe and study many intrinsic properties of the underlying carbon

nanotubes. The functionalization targeting nanotube surface defects (including open ends) seems preserving the nanotube electronic structures much better (Niyogi et al., 2002; Chen et al., 1998).

Experimentally, a typical estimate on the population of defects on the nanotube surface suggests that the defects represent a few percent of the nanotube carbons (Kuznetsova et al., 2000; Hu et al., 2001). After oxidative treatments, these defect nanotube carbons are converted into oxygen-containing groups (especially carboxylic acid moieties). These functional groups on the nanotube surface may be derivatized with a variety of reagents in functionalization reactions. For example, Sun and coworkers have explored many oligomeric and polymeric molecules containing hydroxyl or amino groups for esterification or amidation reactions with the nanotube-bound carboxylic acids (Fig. 6.2) (Sun et al., 2002).

The functionalization of carbon nanotubes with the selected oligomeric or polymeric molecules typically improves dramatically their solubility in common organic solvents and/or water, depending upon the properties of the molecules. For example, solubilities of carbon nanotubes in both water and organic solvents were afforded by the functionalization with $PEG_{1500N}$ (Huang et al., 2003) or PPEI-EI polymer (Fig. 6.2) (Lin et al., 2002). The nanotube-equivalent solubilities for the functionalized carbon nanotubes are usually on the order of a few mg/mL to as high as about 100 mg/mL with the right functional groups and functionalization reactions (Fernando et al., 2004). The soluble functionalized carbon nanotubes are generally in individual nanotubes or thin bundles, which can be probed and visualized by imaging with state-of-the-art electron microscopy techniques (Fig. 6.7) (Lin et al., 2003).

The solubility has allowed the characterization and investigations in the solution phase. For example, nanotube carbons in soluble functionalized sample of SWNTs were recently detected in solution by $^{13}C$ NMR (Kitaygorodskiy et al., 2005). It has also been shown that the solubilization by functionalization targeting defect sites largely preserves the electronic structures and optical transitions in SWNTs, especially the observation that the band-gap absorptions associated with the van Hove singularity pairs are little changed when measured in both solution-phase and the solid state (Fig. 6.8) (Lin et al., 2005; Zhou et al., 2003).

## 6.3.2 Photoluminescence Features and Properties

The solubilization of carbon nanotubes via chemical functionalization has provided great opportunities for studying optical properties of nanotubes in solution phase under the condition of homogeneous dispersion. The most relevant was the discovery by Sun and coworkers that polymer-functionalized carbon nanotubes are luminescent or strongly luminescent in homogeneous organic or aqueous solution, exhibiting broad luminescence emission bands in the visible and well extending into the near-IR region (Fig. 6.9) (Riggs et al., 2000). The luminescence

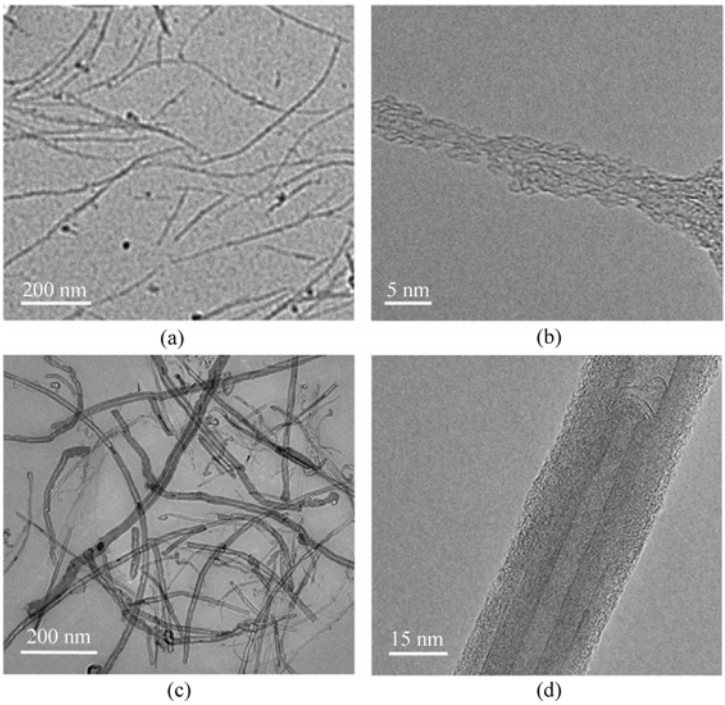


**Figure 6.7** TEM images of (a), (b) a PPEI-EI-functionalized SWNT sample and (c) ,(d) a PI-$NH_2$-f unctionalized MWNT sample

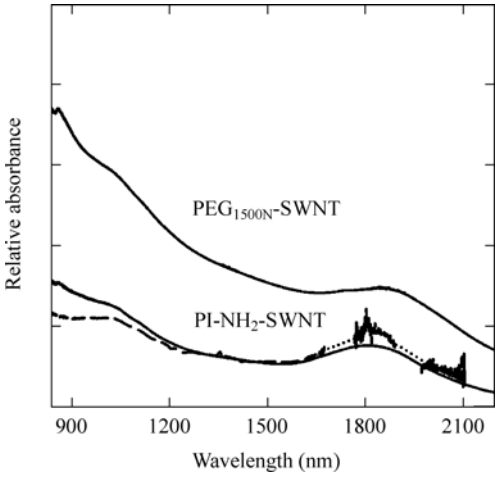


**Figure 6.8** Absorption spectra of $PEG_{1500N}$-SWNT in the solid-state (solid line) and PI-$NH_2$-SWNT in DMF solution (dashed line, the dotted line region subject to overwhelming solvent background) and the solid-state (solid line) (Reproduced from (Lin et al., 2005) with permission. Copyright ©2005 American Chemical Society)

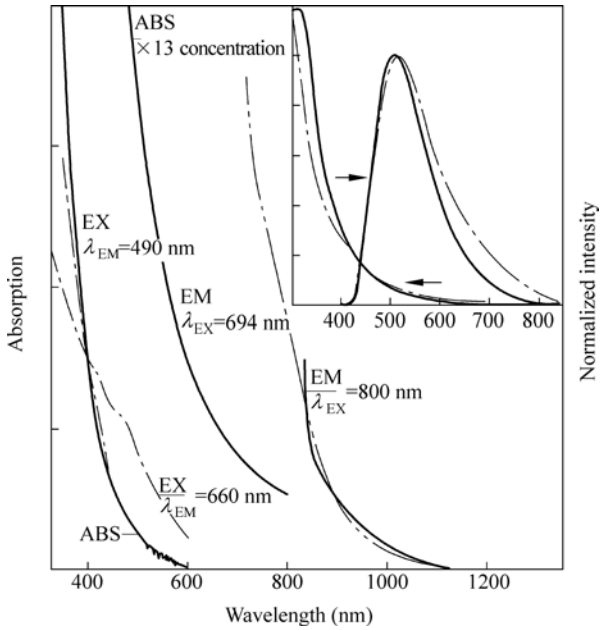


**Figure 6.9** Absorption (ABS), luminescence (EM), and luminescence excitation (EX) spectra of the PPEI-EI-MWNT in room-temperature chloroform. Inset: A comparison of absorption and luminescence (440 nm excitation) spectra of PPEI-EI-MWNT (solid line) and PPEI-EI-SWNT (dashed line) in homogeneous chloroform solutions at room temperature (Reproduced from (Riggs et al., 2000) with permission. Copyright ©2000 American Chemical Society)

of functionalized carbon nanotubes is not specific to any particular polymeric or oligomeric functionality on the nanotube surface. In fact, the luminescence has been observed in all well-functionalized carbon nanotube samples of diverse functional groups (Riggs et al., 2000; Guldi et al., 2002; Banerjee and Wong, 2002; Lin et al., 2005; Sun et al., 2002). Much effort was made to eliminate other possible explanations on the observed strong luminescence emission. For example, fluorescence contribution from the polymers or oligomers used in the functionalization was ruled out because these molecules have no absorption at the excitation wavelength. The possibility of luminescent impurities and small aromatic species induced from the solubilization was also excluded in various control experiments.

The luminescence excitation spectra of functionalized carbon nanotubes monitored at different emission wavelengths are consistent with the broad UV-vis absorption spectra. However, the emission spectra are strongly dependent on excitation wavelengths in a progressive fashion. The excitation wavelength dependence indicates the presence of significant inhomegeneity or a distribution of emitters in the sample (nanotubes of different diameters, in particular) or

emissive excited states (trapping sites of different energies) (Riggs et al., 2000; Banerjee and Wong, 2002; Sun et al., 2002; Lin et al., 2005).

The observed luminescence quantum yields are generally high. As shown in Fig. 6.10, for example, the luminescence quantum yields of PPEI-EI-functionalized SWNTs (PPEI-EI-SWNT) and $PEG_{1500N}$-functionalized SWNTs ($PEG_{1500N}$-SWNT) at 450 nm excitation are 4.5% and 3%, respectively (Lin et al., 2005). Generally speaking, the luminescence quantum yields of SWNTs and MWNTs are on the same order of magnitude. The luminescence decays of functionalized nanotubes are relatively fast and non-exponential, with average lifetimes on the order of a few nanoseconds. The non-exponential nature of the luminescence decays is consistent with the presence of multiple emissive entities in the sample and the observed excitation wavelength dependence of luminescence.

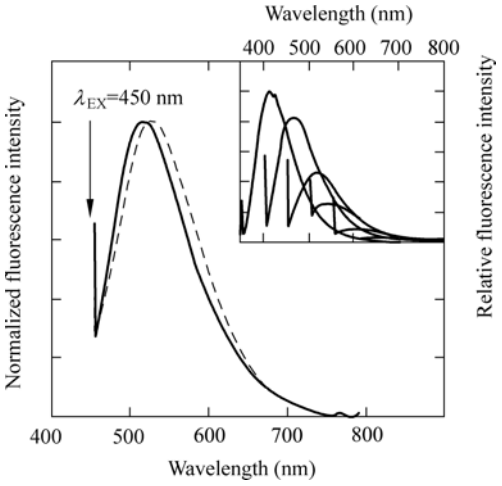


**Figure 6.10** Luminescence emission spectra (normalized, 450 nm excitation) of PPEI-EI-SWNT (solid line) and $PEG_{1500N}$-SWNT (dashed) in aqueous solution. Inset: the spectra of PPEI-EI-functionalized SWNT excited at 350 nm, 400 nm, 450 nm, 500 nm, 550 nm, and 600 nm (intensities shown in relative quantum yields) (Reproduced from (Lin et al., 2005) with permission. Copyright ©2005 American Chemical Society)

### 6.3.2.1 Effect of Dispersion

There is ample experimental evidence suggesting that the defect-derived luminescence is sensitive to the degree of functionalization and dispersion of the carbon nanotubes. The higher observed luminescence quantum yields are generally associated with better functionalized carbon nanotubes, as supported by results from the experiments of repeated functionalization and the defunctionalization of functionalized carbon nanotubes (Lin et al., 2005; Sun et al., 2002). The repeated functionalization reactions of a carbon nanotube sample with the same polymer results in a substantial increase in the luminescence quantum

yield of the final functionalized nanotube sample. Conversely, the luminescence can be quenched or eliminated upon partial or complete defunctionalization process through thermal evaporation or acid/base hydrolysis to remove the functional groups from the nanotube surface. The polymer-functionalized carbon nanotube samples obtained from different functionalization routes may have different luminescence quantum yields due to the nature of the functionalization reactions with respect to the nanotube dispersion. It is commonly observed that the amidation/esterification of carbon nanotubes through the acyl chloride route (Chen et al., 1998; Lin et al., 2002) is more effective than other reactions (such as the diimide-activated coupling (Huang et al., 2002) in the functionalization, corresponding to a higher degree of nanotube dispersion in the resulting sample.

The functionalization of carbon nanotubes for their solubilization is likely more than just dragging the nanotubes into aqueous or common organic solution through covalently wrapping the nanotube with the oligomeric or polymeric molecules. In the functionalization reaction, the functional groups exfoliate the nanotube bundles by either reducing the bundle size or completely disintegrating the bundle into individual nanotubes (thus, the degree of nanotube dispersion greatly enhanced) (Lin et al., 2003). Better functionalized carbon nanotubes and the associated better dispersion result in higher luminescence quantum yields. Conversely, stronger luminescence serves as an indication that the underlying nanotubes are better dispersed, which may be verified or supported by other complementary techniques such as high-resolution electron microscopy or atomic force microscopy. In fact, because of the sensitivity of fluorescence spectroscopy, the luminescence measurements may be used as an experimental tool for probing the dispersion of carbon nanotubes.

Lin, et al. have demonstrated the sensitivity of the defect-derived luminescence to the nanotube dispersion (Lin et al., 2005). In a comparison of non-functionalized and functionalized SWNTs, the former were dispersed in DMF with the assistance of polyimide under sonication. The latter (SWNTs functionalized with polyimide) were dissolved in DMF to afford another solution. At the same equivalent nanotube content, the two solutions had comparable optical density at the same excitation wavelength (450 nm). However, the luminescence measurements of the two solutions revealed that the latter was much more luminescent than the former (Fig. 6.11). This is a piece of evidence strongly in support of the conclusion that the dispersion of carbon nanotubes plays a critical role in their luminescence.

The effective exfoliation to obtain individually dispersed nanotubes is a necessary prerequisite to observe strong defect-derived luminescence. This requirement seems the same as that for the detection of band-gap fluorescence (O'Connell et al., 2002) because both emissions are subject to the inter-nanotube quenching effect. Again, the high quantum yield of defect-derived luminescence combined with the sensitivity to nanotube bundling may be exploited as a convenient, effective, and non-invasive technique to monitor the dispersion of carbon nanotubes

in polymer and other matrices.

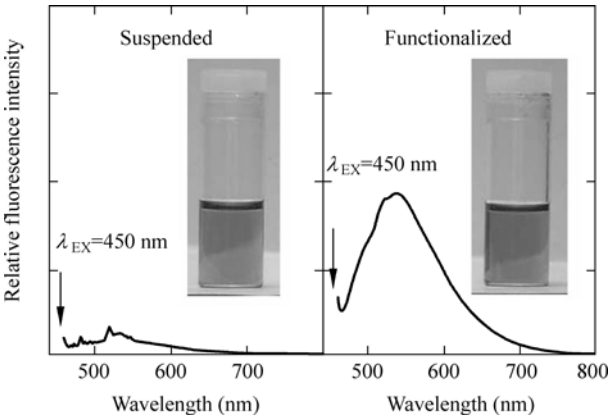


**Figure 6.11** Luminescence emission spectra and pictures from SWNTs dispersed with the aid of polyimide in DMF (a) and the PI-$NH_2$- SWNT in DMF solution (b). The nanotube and polymer contents in the two samples were comparable (Reproduced from (Lin et al., 2005) with permission. Copyright ©2005 American Chemical Society)

### 6.3.2.2 Effect on Raman

The strong luminescence in functionalized carbon nanotubes often becomes overwhelmingly interfering in the Raman characterization of the nanotube samples. Resonant Raman spectroscopy has been identified as one of the most important experimental tools for probing and studying carbon nanotubes because of the sensitivity of Raman features to the nanotube diameter, chirality, environmental effect, etc. For example, a typical Raman spectrum of a pristine SWNT sample shows characteristic peaks including the radial breathing mode (100 – 300 $cm^{-1}$), D-band (~1300 $cm^{-1}$), G-band (~1600 $cm^{-1}$), and D*-band (~2600 $cm^{-1}$). However, for functionalized carbon nanotubes, these characteristic Raman bands are generally obscured or overwhelmed by the strong luminescence background, which essentially turns the Raman spectrum into a luminescence spectrum (Lin et al., 2005; Sun et al., 2002). The extent of luminescence interference in Raman measurements is consistent with the intensities in directly measured luminescence spectra. Better-functionalized nanotube samples with better solubility and dispersion are usually associated with more intensive luminescence interference, which often buries the Raman features completely. For example, the Raman spectrum of Ⅰ-MWNT is simply a broad curve (Fig .6.12) (Sun et al., 2002).

The luminescence background in Raman spectra could be removed by reducing the degree of nanotube functionalization. Typically, a chemical or thermal defunctionalization process may be used to remove the functional groups from the nanotube surface. The characteristic Raman features of carbon nanotubes are restored upon the defunctionalization, as shown in Fig. 6.12 for Ⅰ-MWNT.

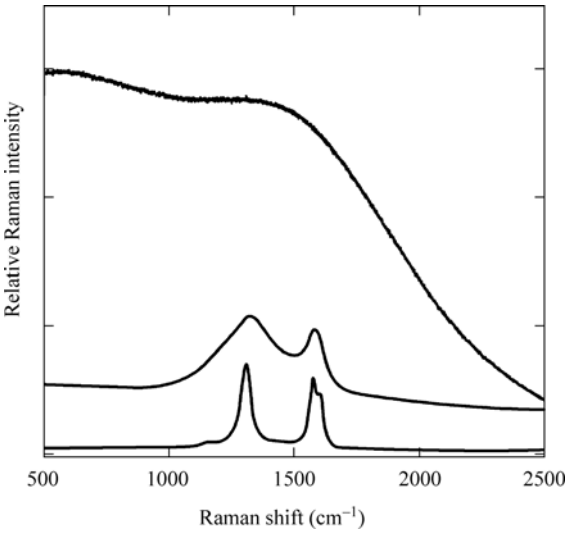


**Figure 6.12** Raman spectra (785 nm excitation) of the Ⅰ-MWNT sample (Fig. 6.2) before (top) and after (middle) thermal defunctionalization in a TGA scan to 650℃. The spectrum of the pristine MWNT sample (bottom) is also shown for comparison (Reproduced from (Sun et al., 2002) with permission. Copyright ©2002 American Chemical Society)

### 6.3.3 Defect-Derived vs Band-Gap Emissions

The two emissions of carbon nanotubes are obviously different in origin, but complementary in some properties. As observed by Kappes, et al. in the measurement of band-gap fluorescence, there was a significantly stronger and structureless luminescence background toward the visible region with the intensity increasing smoothly toward the excitation wavelength for stable dispersion of acid-treated SWNTs (Lebedkin et al., 2003a). It suggests the coexistence of the two kinds of emissions in the same carbon nanotube sample.

The band-gap emission is likely much weaker and very sensitive to any effects on the electronic structure of SWNTs (easily quenched or diminished by doping or chemical treatment). For example, the emission spectrum of dispersed SWNTs after the acid-treatment is weak and poorly structured (Lebedkin et al., 2003a). However, the defect-derived luminescence is much improved by the same procedure that induces or generates more defects sites. The excellent surface passivation is critical to the observation of strong defect-derived luminescence (Lin et al., 2005).

The band-gap emission is strongly dependent on the nanotubes diameter $d$ and diameter distribution (O'Connell et al., 2002; Lebedkin et al., 2003a). It has been reported that the quantum efficiency of SWNTs from the arc-discharge production ($d \sim 1.5$ nm) are weaker in band-gap fluorescence because of their larger average diameter than that of SWNTs produced from the HiPco method ($d \sim 0.7 - 1.2$ nm) (Lebedkin et al., 2003a). The band-gap emission is more prominent in the

small-diameter nanotubes with an upper diameter limit of 1.5 nm. For example, the observed quantum yield of SWNTs from the laser ablation production ($d \sim 1.4$ nm) is on the order of $1\times10^{-5}$, two orders of magnitude lower than that of the HiPco nanotubes. SWNTs from arc-discharge are predicted to have an even lower quantum yield, which may actually represent a technical challenge in the observation of their band-gap fluorescence.

A shared requirement between the two kinds of emissions is that the emission is highly sensitive to the nanotube dispersion. For the band-gap emission, the dispersion is often assisted by the use of surfactants with the carbon nanotubes and also ultra-high-speed centrifugation. The functionalization is effective in the exfoliation of nanotubes bundles to the level of individual nanotubes and very thin bundles, but it is hardly applicable to the investigation of band-gap fluorescence. Despite the extensive effort on the elucidation of the two kinds of emissions, there are still significant technical and mechanistic issues for both. For example, the accurate determination of quantum yield for the band-gap fluorescence remains difficult because of the wavelength region, while the nature and properties of the emissive excited states for the defect-derived luminescence require further investigations.

## 6.4 Dots vs Tubes—Luminescence Polarization

A significant difference in the photoluminescence properties of carbon dots vs carbon nanotubes is in their different polarization characteristics. The luminescence emissions of carbon dots with oligomeric passivation agents on the dot surface are hardly polarized in solution (Zhou and Sun, unpublished). However, the luminescence emissions of functionalized carbon nanotubes are highly polarized both in solution at ambient temperature and in polymer thin films. The anisotropy values $r$ can be calculated for the nanotube luminescence in terms of the well-established equations (Lakowicz, 1999).

$$P = (I_{HH}I_{VV} - I_{HV}I_{VH})/(I_{HH}I_{VV} + I_{HV}I_{VH}) \tag{6.1}$$

$$r = 2P/(3-P) \tag{6.2}$$

At each excitation wavelength, the anisotropy values are essentially independent of emission wavelengths. Shown in Fig. 6.13 are typical luminescence anisotropy results for the functionalized SWNTs, where each value is averaged over all emission wavelengths (Sun et al., 2002).

The luminescence anisotropy values are strongly dependent on the excitation wavelengths, exhibiting obvious increases with progressively longer excitation wavelengths, approaching the limiting anisotropy value of 0.4 (Table 6.1). The excitation wavelength dependence of the anisotropy value is less significant in polymer films than in solution (Zhou et al., 2006).

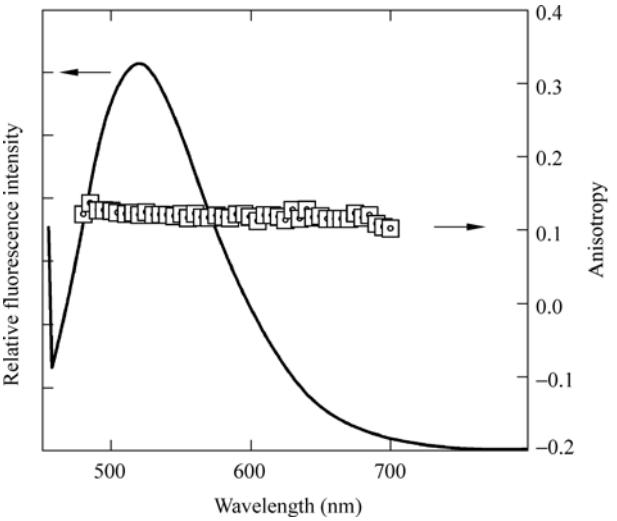


**Figure 6.13** Luminescence anisotropy values at different emission wavelengths for $I_{PEG}$-MWNT (Fig. 6.2) in room-temperature chloroform solution with 450 nm excitation. The luminescence spectrum at the same excitation wavelength is also shown for comparison (Reproduced from (Sun et al., 2002) with permission. Copyright ©2002 Elsevier Science B.V.)

**Table 6.1** Luminescence anisotropy ($r$) values at different excitation wavelengths (Zhou et al., 2006)

| Excitation Wavelength (nm) | $r_{solution}$ [(1)] | $r_{film}$ | Excitation Wavelength (nm) | $r_{solution}$ [(1)] | $r_{film}$ |
|---|---|---|---|---|---|
| 400 | 0.052 | 0.32 | 525 | 0.15 | 0.38 |
| 425 | 0.069 | 0.34 | 550 | 0.16 | 0.39 |
| 450 | 0.10 | 0.35 | 575 | 0.18 | 0.39 |
| 475 | 0.12 | 0.35 | 600 | 0.19 | 0.39 |
| 500 | 0.14 | 0.37 | | | |

[(1)] From repeating the experiments reported in ref (Sun et al., 2006).

The luminescence emission is likely associated with excited state energy trapping sites (well-passivated nanotube surface defects). The luminescence polarization indicates that the absorption and emission dipole moments are correlated. The excitation wavelength dependence of luminescence polarization seems to suggest that the excitation is at least partially localized in a distribution of electronic states in the functionalized carbon nanotubes. For the functionalized carbon nanotubes embedded in the polymeric matrix, the anisotropy values are generally larger than those in solution. This may be attributed to the more restrictive environment in the films toward rotational diffusion, thus minimizing or completely eliminating the depolarization induced by molecular motion.

The absorption and emission dipole moments are close to being parallel for the functionalized carbon nanotubes dispersed in the polymeric matrix. However, the orientation of parallel dipoles with respect to the nanotube structure can not be revealed from only the luminescence anisotropy results. The alignment of the luminescent carbon nanotubes is required. The alignment has been achieved by uniaxial mechanic stretching of PVA thin films embedded with functionalized SWNTs. The large aspect ratio of carbon nanotubes makes them good candidates for the alignment by mechanical stretching, as already reported in the literature (see, for example, (Rozhin et al., 2005)). Experimentally, the nanotube-embedded PVA films (about 100 microns in thickness) can usually be stretched to 5 – 7 fold. The observed dichroic ratios are strongly in favor of the film stretching direction (Fig. 6.14), indicating that the electronic absorption responsible for the luminescence properties are along the nanotube long axis (Zhou et al., 2006). When combined with the luminescence anisotropy results, an obvious conclusion is that both the absorption and emission dipole moments are coaxial with the functionalized carbon nanotubes. It should be noted that the measurement of luminescence emissions from the stretched films is a more sensitive alternative to the direct determination of absorption polarization in reference to the film stretching direction.

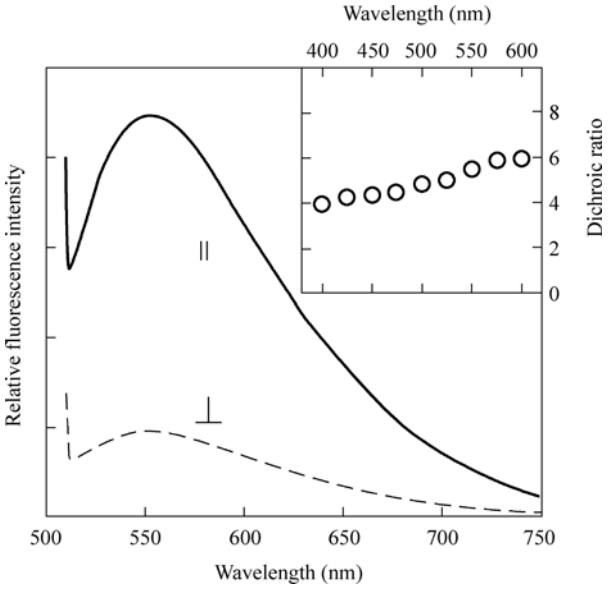


**Figure 6.14** Luminescence emission spectra of PPEI-EI-SWNT in stretched PVA film (draw ratio ~ 5) excited with polarized light parallel (||, solid line) and perpendicular (⊥, dashed line) to the stretching direction. Shown in the inset is the excitation wavelength dependence of the observed dichroic ratio (Reproduced from (Zhou et al., 2006) with permission. Copyright ©2006 American Chemical Society)

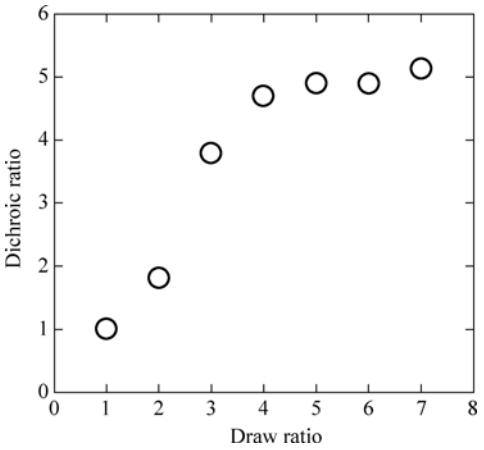


**Figure 6.15** The observed dichroic ratio for PPEI-EI-SWNT in stretched PVA film as a function of the draw ratio (500 nm excitation) (Reproduced from (Zhou et al., 2006) with permission. Copyright ©2006 American Chemical Society)

The alignment of the functionalized SWNTs in the stretched PVA film has also been evaluated in terms of the dependence of the observed dichroic ratio on the draw ratio (Zhou et al., 2006). As shown in Fig. 6.15 for the stretching with the film draw ratio from 1 to 7, the dichroic ratio initially increases rapidly with the increasing draw ratio and then reaches almost a plateau.

Further investigations on the similarities and differences between photoluminescence properties of carbon dots and functionalized carbon nanotubes are in progress.

## 6.5 Potential Applications

Most excitements generated by fluorescent quantum dots (QDs) are for their potential applications in biological and medical sciences, such as bio-tagging and bio-imaging (Michalet et al., 2005; Park et al., 2003, 2005; Alivisatos et al., 2005; Alivisatos, 2004; Fu et al., 2005; Gao et al., 2004). However, there are many serious concerns on traditional QDs, especially those based on cadmium and lead, for their toxicity both in vitro and in vivo (Michalet et al., 2005; Derfus et al., 2004; Kirchner et al., 2005; Holmes et al., 2000). Recent results suggest that the photoluminescent carbon dots may serve as competitive alternatives to the traditional QDs in similar bio-applications. For example, Sun and coworkers used water-soluble $PEG_{1500N}$-passivated carbon dots to label Escherichia coli (E. coli) cells (Fig. 6.16) and Bacillus subtilis spores (commonly used simulant for anthrax spores, Fig. 6.17) (Sun et al., 2006).

The bright photoluminescence in functionalized carbon nanotubes may find similar bio-tagging and bio-imaging applications, as demonstrated by the existing

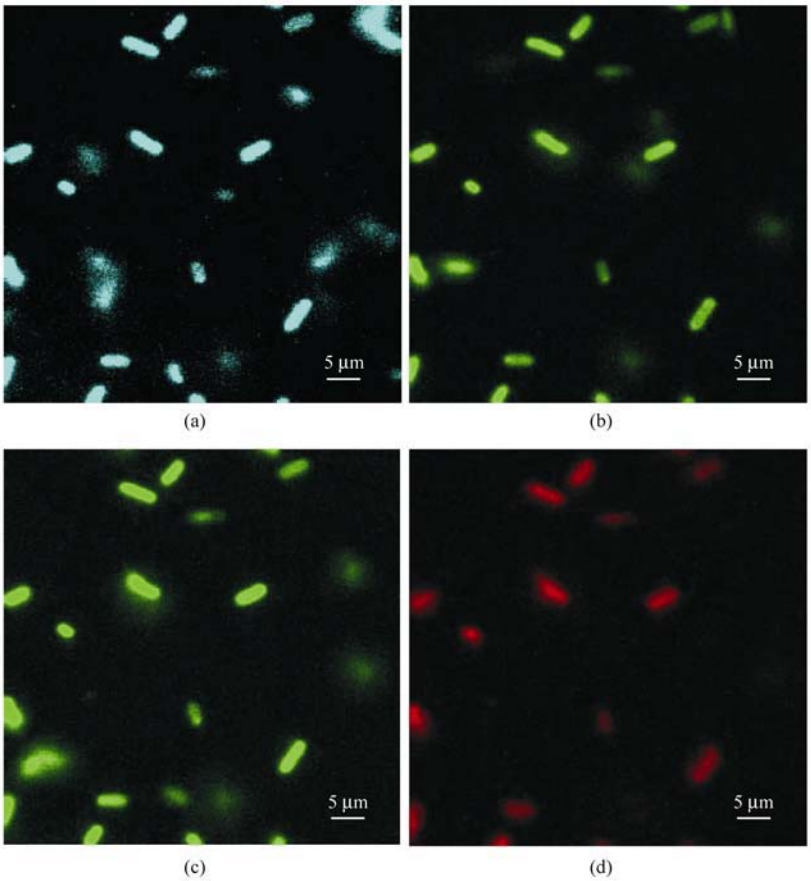


**Figure 6.16** Confocal microscopy images of E. coli ATCC 25922 cells labeled with luminescent carbon dots (Color Fig.15): (a) $\lambda_{EX}$ = 458 nm, detected with 475 nm long pass filter; (b) $\lambda_{EX}$ = 477 nm, detected with 505 nm long pass filter; (c) $\lambda_{EX}$ = 488 nm, detected with 530 long pass filter (d) $\lambda_{EX}$ = 514 nm, detected with 560 nm long pass filter (Reproduced from (Sun et al., 2006) with permission. Copyright © 2006 American Chemical Society)

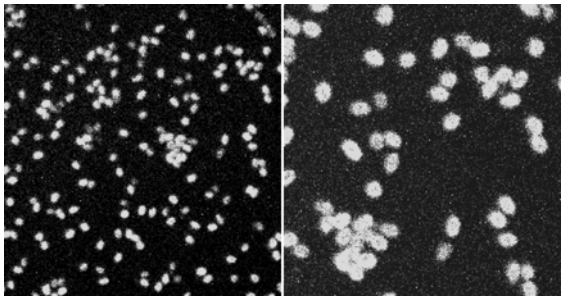

**Figure 6.17** Confocal microscope images of Bacillus subtilis spores labeled with luminescent carbon dots ( $\lambda_{EX}$ = 488 nm, detected with 545 nm neutral density long pass filter)

confocal imaging results on the evaluation of polymeric nanocomposite materials (Zhou et al., 2006). Shown in Fig. 6.18 are confocal microscopy images of the PVA film dispersed with PPEI-EI-SWNT. The images at different depths beneath the film surface suggest that these are representative of the whole film matrix (not any surface effects). The compatibility of the functionalized nanotubes with and their well-dispersion in the PVA matrix are also reflected in the confocal images, with bright and homogeneous emissions (spatial resolution about 0.5 μm)

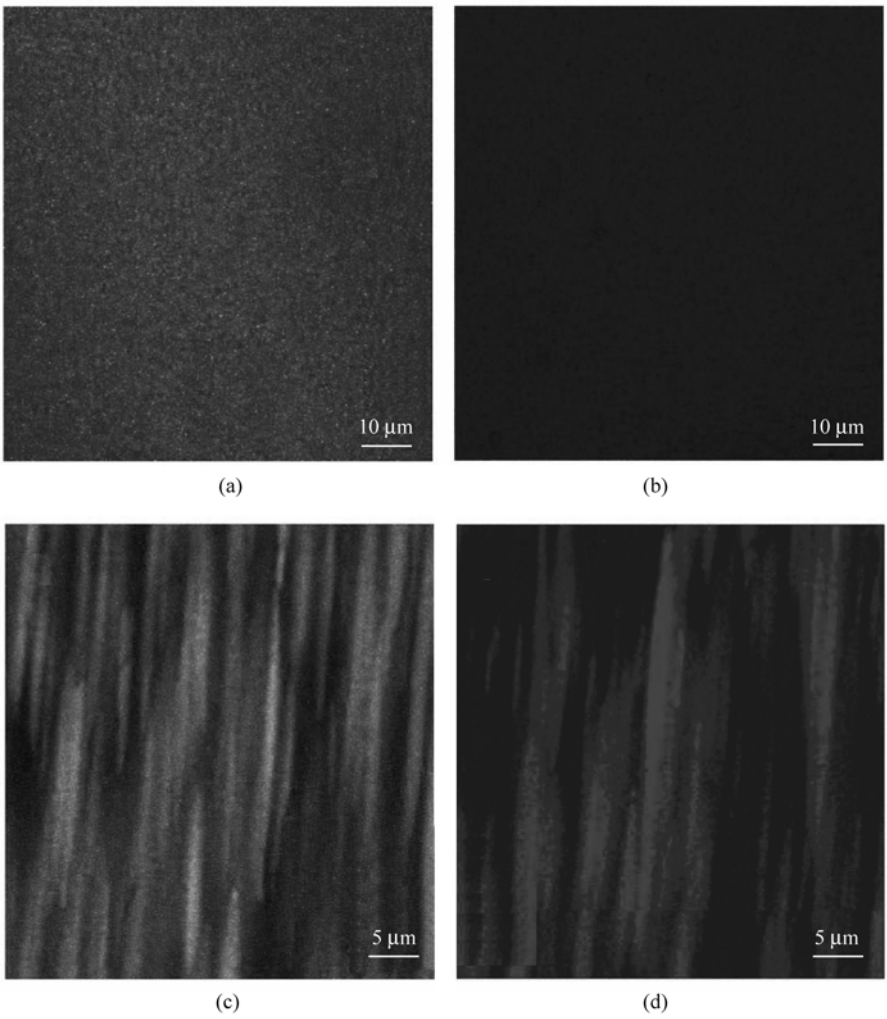


**Figure 6.18** Confocal microscopy images of PPEI-EI-SWNT in PVA film (Color Fig. 16) (a), (b) before and (c), (d) after mechanical stretching to a draw ratio of about 5. (a), (c) 514 nm excitation, >530 nm detection; (b), (d) 633 nm excitation, >650 nm detection (Reproduced from (Zhou et al., 2006) with permission. Copyright © 2006 American Chemical Society)

across the whole film. The emission light intensity as expressed by the color intensity from across the film is uniform, without obvious deviation (such as bright or dark spots from local aggregation, locally enrichment or absence of functionalized nanotubes, etc.). Different excitation wavelengths can be used (such as 514 nm and 633 nm in Fig. 6.18). For the stretched films, while the nanotubes remain well-dispersed according to confocal microscopy images (Fig. 6.18), their preferential orientation along with the stretching direction is also well illustrated in the images.

The conceptually similar material configuration can obviously be applied to the fluorescence microscopy imaging of biological systems. In this regard, carbon dots and specifically functionalized carbon nanotubes serve as luminescence agents of somewhat different characteristics, mostly physical such as dramatically different aspect ratios and optical polarizations, but also potentially biological in their interactions with bio-systems.

## Acknowledgement

Financial support from NSF, NASA, USDA, ONR, Center for Advanced Engineering Fibers and Films (NSF-ERC at Clemson University), and South Carolina Space Grant is gratefully acknowledged.

## References

Special issue on carbon nanotubes. *Acc. Chem. Res.* **35** (2002).

Dresselhaus, M.S. and H.J. Dai. *Theme: Advances in Carbon Nanotubes, MRS Bull vol* **29** (2004)

Baughman, R.H., A.A. Zakhidov and D.H. de Heer. *Science* **297**: 787 (2002).

Dresselhaus. M.S., G. Dresselhaus and P.C. Eklund. *Science of Fullerenes and Carbon Nanotubes.* New York: Academic Press (1996).

Kataura, H., Y. Kumasawa, Y. Maniwa, I. Umezu, S. Suzuki, Y. Ohtsuka and Y. Achiba *Synth. Met*. **103**: 2555 (1999).

O'Connell, M.J., S.M. Bachilo, C.B. Huffman, V.C. Moore, M.S. Strano, E.H. Haroz, K.L. Rialon, P.J. Boul, W.H. Noon, C. Kittrell, J. Ma, R.H. Hauge, R.B. Weisman and R.E. Smalley. *Science* **297**: 593 (2002).

Bachilo, S.M., M.S. Strano, C. Kittrell, R.H. Hauge, R.E. Smalley and R.B. Weisman. *Science* **298**: 2361 (2002).

Lebedkin, S., F. Hennrich, T. Skipa and M.M. Kappes. *J. Phys. Chem. B* **107**: 1949 (2003a).

Lebedkin, S., K. Arnold, F. Hennrich, R. Krupke, B. Renker and M.M. Kappes. *New. J. Phys.* **5**: 140 (2003b).

Jones, M., C. Engtrakul, W.K. Metzger, R.J. Ellingson, A.J. Nozik, M.J. Heben and G.P. Rumbles. *Phys. Rev. B* **71**: 115,426 (2005).

Graff, R.A., J.P. Swanson, P.W. Barone, S. Baik, D.A. Heller and M.S. Strano. *Adv. Mater.* **17**: 980 (2005).

Lefebvre, J., J.M. Fraser, P. Finnie and Y. Homma . *Phys. Rev. B* **69**: 075,403 (2004).

Hennrich, F., R. Krupke, S. Lebedkin, K. Arnold, R. Fischer, D.E. Resasco and M.M. Kappes. *J. Phys. Chem. B* **109**: 10,567 (2005).

Arnold, K., S. Lebedkin, O. Kiowski, F. Hennrich and M.M. Kappes. *Nano. Lett.* **4**: 2349 (2004).

Riggs, J.E., Z. Guo, D.L. Carroll and Y.P. Sun. *J. Am. Chem. Soc.* **122**: 5879 (2000).

Zhao, B., H. Hu, S. Niyogi, M.E. Itkis, M.A. Hamon, P. Bhowmik, M.S. Meier and R.C. Haddon. *J. Am. Chem. Soc.* **123**: 11,673 (2001).

Guldi, D.M., M. Holzinger, A. Hirsch, V. Georgakilas and M. Prato. *Chem. Commun.* 1130 (2003).

Banerjee, S. and S.S.Wong. *J. Am. Chem. Soc.* **124**: 8940 (2002).

Sun, Y.P., B. Zhou, K. Henbest, K. Fu, W. Huang, Y. Lin, S. Taylor and D.L. Carroll. *Chem. Phys. Lett*. **351**: 349 (2002).

Lin, Y., B. Zhou, R.B. Martin, K.B. Henbest, B.A. Harruff, J.E. Riggs, Z.X. Guo, L.F. Allard and Y.P. Sun. *J. Phys. Chem. B* **109**: 14,779 (2005).

Sun, Y.P., B. Zhou, Y. Lin, W. Wang, K.A.S. Fernando, P. Pathak, M.J. Meziani, B.A. Harruff, X.Wang, H.F. Wang, P.J.G. Luo, H. Yang, M.E. Kose, B.L. Chen, L.M. Veca and S.Y. Xie. *J. Am. Chem. Soc*. **128**: 7756 (2006).

Chan, W.C.W and S. Nie. *Science* **281**: 2016 (1998).

Klimov, V.I., A.A. Mikhailovsky, S. Xu, A. Malko, J.A. Hollingsworth, C.A. Leatherdale, H.J. Eisler and M.G. Bawendi. *Science* **290**: 314 (2000).

Bruchez, M., M. Moronne, P. Gin, S. Weiss and A.P. Alivisatos. *Science* **281**: 2013 (1998).

Esteves, A.C.C. and T. Trindade. *Curr. Opin. Solid. State Mater. Sci.* **6**: 347 (2002).

Green, M. *Curr. Opin. Solid. State Mater. Sci.* **6**: 355 (2002).

Alivisatos, A.P. *Science* **271**: 933 (1996).

Larson, D.R., W.R. Zipfel, R.M. Williams, S.W. Clark, M.P. Bruchez, F.W. Wise and W.W. Webb. *Science* **300**: 1434 (2003).

Michalet, X., F.E. Pinaud, L.A. Bentolila, J.M. Tsay, S. Doose, J.J. Li, G. Sundaresan, A.M. Wu, S.S. Gambhir and S. Weiss. *Science* **307**: 538 (2005).

Parak, W.J., D. Gerion, T. Pellegrino, D. Zanchet, C. Micheel, S.C. Williams, R. Boudreau, M. A. Le Gros, C.A. Larabell and A.P. Alivisatos. *Nanotechnology* **14**: R15 (2003).

Medintz, I.L., H.T. Uyeda, E.R. Goldman and H. Mattoussi. *Nat. Mater.* **4**: 435 (2005).

Kim, S., Y.T. Lim, E.G. Soltesz, A.M. De Grand, J. Lee, A. Nakayama, J.A. Parker, T. Mihaljevic, R.G. Laurence, D.M. Dor, L.H. Cohn, M.G. Bawendi and J.V. Frangioni. *Nat. Biotechnol*. **22**: 93 (2003).

Ding, Z.F., B.M. Quinn, S.K. Haram, L.E. Pell, B.A. Korgel and A.J. Bard. *Science* **296**: 1293 (2002).

Chen, C.S., J. Yao and R.A. Durst. *J. Nanopart. Res.* **8**: 1033 (2006).

Bharali, D.J., D.W. Lucey, H. Jayakumar, H.E. Pudavar and P.N. Prasad. *J. Am. Chem. Soc.* **127**: 11,364 (2005).

Seydack, M. *Biosens. Bioelectron*. **20**: 2454 (2005).

Wilson, W.L., P.F. Szajowski and L.E. Brus. *Science* **262**: 1242 (1993).

Burns, A., H. Ow and U. Wiesner. *Chem. Soc. Rev.* **35**: 1028 (2006).

Derfus, A.M., W.C.W. Chan and S.N. Bhatia. *Nano Lett*. **4**: 11 (2004).

Kirchner, C., T. Liedl, S. Kudera, T. Pellegrino, A.M. Javier, H.E. Gaub, S. Stolzle, N. Fertig and W.J. Parak. *Nano Lett*. **5**: 331 (2005).

Lovric, J., S.J. Cho, F.M. Winnik and D. Maysinger. *Chem. Biol*. **12**: 1227 (2005).

Holmes, J.D., K.P. Johnston, C. Doty and B.A. Korgel. *Science* **287**: 1471 (2000).

Belomoin, G., J. Therrien, A. Smith, S. Rao, R. Twesten, S. Chaieb, M.H. Nayfeh, L. Wagner and L. Mitas. *Appl. Phys. Lett*. **80**: 841 (2002).

Hua, F., M.T. Swihart and E. Ruckenstein. *Langmuir*. **21**: 6054 (2005).

Li, Z.F. and E. Ruckenstein. *Nano Lett.* **4**: 1463 (2004).

Huisken, F., G. Ledoux, O. Guillos and C. Reynaud. *Adv. Mater*. **14**: 1861 (2002).

Lin, Y., D.E. Hill, J. Bentley, L.F. Allard and Y.P. Sun. *J. Phys. Chem*. *B* **107**: 10,453 (2003).

Kuno, M., D.P. Fromm, H.F. Hamann, A. Gallagher and D.J. Nesbitt. *J. Chem. Phys*. **115**: 1028 – 1040 (2001).

Shimizu, K.T., R.G. Neuhauser, C.A. Leatherdale, S.A. Empedocles, W.K. Woo and M. G. Bawendi. *Phys. Rev. B* **63**: 205,316 (2001).

Kuno, M., D.P. Fromm, A. Gallagher, D.J. Nesbitt, O.I. Micic, A.J. Nozik. *Nano Lett*. **1**: 557 (2001).

Sychugov, I., R. Juhasz, J. Linnros and J. Valenta. *Phys. Rev. B* **71**: 115,331 (2005).

Geddes, C.D., A. Parfenov, I. Gryczynski and J.R. Lakowicz *Chem. Phys. Lett*. **380**: 269 (2003).

Sun, Y.P., K. Fu, Y. Lin and W. Huang. *Acc. Chem. Res*. **35**: 1096 (2002).

Kose, M.E., B.A. Harruff, Y. Lin, L.M. Veca, F.S. Lu and Y.P. Sun. *J. Phys. Chem. B* **110**: 14,032 (2006).

Zhou, B., Y. Lin, L.M. Veca, K.A.S. Fernando, B.A. Harruff and Y.P. Sun. *J. Phys. Chem. B* **110**: 3001 (2006).

Bahr, J.L., E.T. Mickelson, M.J. Bronikowski, R.E. Smalley and J.M. Tour. *Chem. Commun* 193 (2001).

Bahr, J.L. and J.M. Tour. *J. Mater. Chem*. **12**: 1952 (2002).

Hirsch, A. *Angew. Chem. Int. Ed*. **41**: 1853 (2002).

Tasis, D., N. Tagmatarchis, V. Georgakilas and M. Prato. *Chem. A. Euro. J.* **9**: 4001 (2003).

Niyogi, S., M.A. Hamon, H. Hu, B. Zhao, P. Bhowmik, R. Sen, M.E. Itkis and R.C. Haddon. *Acc. Chem. Res*. **35**: 1105 (2002).

Chen, J., M.A. Hamon, H. Hu, Y. Chen, A.M. Rao, P.C. Eklund and R.C. Haddon. *Science* **282** :95 (1998).

Kuznetsova, A., D.B. Mawhinney, V. Naumenko, J.T. Yates, J. Liu and R.E. Smalley. *Chem. Phys. Lett*. **321**: 292 (2000).

Hu, H., P. Bhowmik, B. Zhao, M.A. Hamon , M.E. Itkis and R.C. Haddon. *Chem. Phys. Lett.* **345**: 25 (2001).

Huang, W.J., S. Fernando, L.F. Allard and Y.P. Sun. *Nano Lett*. **3**: 565 (2003).

Lin, Y., A.M. Rao, B. Sadanadan, E.A. Kenik and Y.P. Sun. *J. Phys. Chem. B* **106**: 1294 (2002).

Fernando, K.A.S., Y. Lin and Y.P. Sun. *Langmuir* **20**: 4777 (2004).

Kitaygorodskiy, A., W. Wang, S.Y. Xie, Y. Lin, K.A.S. Fernando, X. Wang, L.W. Qu, B. Chen and Y.P. Sun. *J. Am. Chem. Soc*. **127**: 7517 (2005).

Zhou, B., Y. Lin, H. Li, W. Huang, J.W. Connell, L.F. Allard and Y.P. Sun. *J. Phys. Chem. B* **107**: 13,588 (2003).

Huang, W., Y. Lin, S. Taylor, J. Gaillard, A.M. Rao and Y.P. Sun. *Nano Lett*. **2**: 231 (2002).

Zhou, B. and Y.P. Sun, et al. Unpublished.

Lakowicz, R.J. *Principles of Fluorescence Spectroscopy*, *2nd edn*. New York: Kluwer Academic/Plenum Publisher (1999).

Rozhin, A.G., Y. Sakakibara, H. Kataura, S. Matsuzaki, K. Ishida, Y. Achiba and M. Tokumoto. *Chem. Phys. Lett*. **405**: 288 (2005).

Parak, W.J., T. Pellegrino and C. Plank. *Nanotechnology* **16**: R9 (2005).

Alivisatos, P. *Nature Biotechnol.* **22**:47 (2004).

Alivisatos, A.P., W.W. Gu, and C. Larabell. *Annu. Rev. Biomed. Eng*. **7**: 55 (2005).

Fu, A.H., W.W. Gu, C. Larabell and A.P. Alivisatos. *Curr. Opin. Neurobiol*. **15**: 568 (2005).

Gao, X., Y. Cui, R.M. Levenson, L.W.K. Chung and S. Nie. *Nat. Biotechnol*. **22**: 969 (2004).